Article

Static and Dynamic Analysis of Conductor Rail with Large Cross-Sectional Moment of Inertia in Rigid Catenary Systems

Xiaohe Feng [1,2], Shibin Gao [1,2], Yang Song [3,4,*] , Zeyao Hu [1], Long Chen [1] and Tao Liang [1]

1   Key Laboratory of Magnetic Suspension Technology and Maglev Vehicle, Ministry of Education, Southwest Jiaotong University, Chengdu 610031, China
2   National Rail Transit Electrification and Automation Engineering Technique Research Centre, Southwest Jiaotong University, Chengdu 610031, China
3   State Key Laboratory of Traction Power, Southwest Jiaotong University, Chengdu 610031, China
4   Department of Built Environment, Oslo Metropolitan University, 7491 Oslo, Norway
*   Correspondence: y.song_ac@hotmail.com

Abstract: The rigid catenary system is widely used in tunnels to power electric trains via contact with a pantograph. Due to gravity, the contact wire normally has a sag that may affect the dynamic interaction performance with a pantograph. To reduce the contact wire sag, the most efficient measure is to improve the moment of inertia of the conductor rail, which is used to clamp the contact wire. Six new types of conductor rail with large moments of inertia are developed based on a conventional conductor rail. Then both the static and dynamic analyses are conducted to investigate the performance of the new types of conductor rail with a big moment of inertia. The conductor rail's 3D solid finite element model is built using a finite element approach. The vertical deflection and the stress distribution are comparatively analyzed among different types of conductor rail. The analysis results indicate that the vertical deflection and maximum stress are significantly reduced when using the conductor rail with a large moment of inertia. The best performance is observed when the conductor rail of case 1 is used. The maximum sag is reduced by 28.37%, and the maximum stress is decreased by 27.76% compared with the conventional conductor. Finally, a pantograph model is included to evaluate the dynamic performance of the conductor rail with large moments of inertia. The results indicate that contact force fluctuation is significantly reduced after the conductor rails with large moments of inertia are presented. The conductor rail of case 1 shows the best performance, which can reduce the contact force standard deviation by 32% and 27% at speeds of 160 km/h and 200 km/h.

Keywords: rigid catenary; pantograph; conductor rail; large moment of inertia; electrified railway

1. Introduction

In electric railways, the rigid catenary is widely adopted in tunnels to power the train (Figure 1a). Compared with the traditional soft catenary, the rigid catenary is much easier to mount on the tunnel's roof. The rigid catenary normally comprises the contact wire, conductor rail, and brackets (Figure 1b). Compared with the soft catenary, the rigid catenary is simple, robust, easy to maintain, and has better resistance to environmental disturbances, such as wind load. At present, the rigid catenary has been the mainstream selection of the current collection solution in urban underground metro lines as the soft catenary makes it difficult to satisfy the requirement of the lower installation height in tunnels [1,2]. The static and dynamic behavior of the rigid catenary is beginning to attract ever-increasing attention from academia and industry.
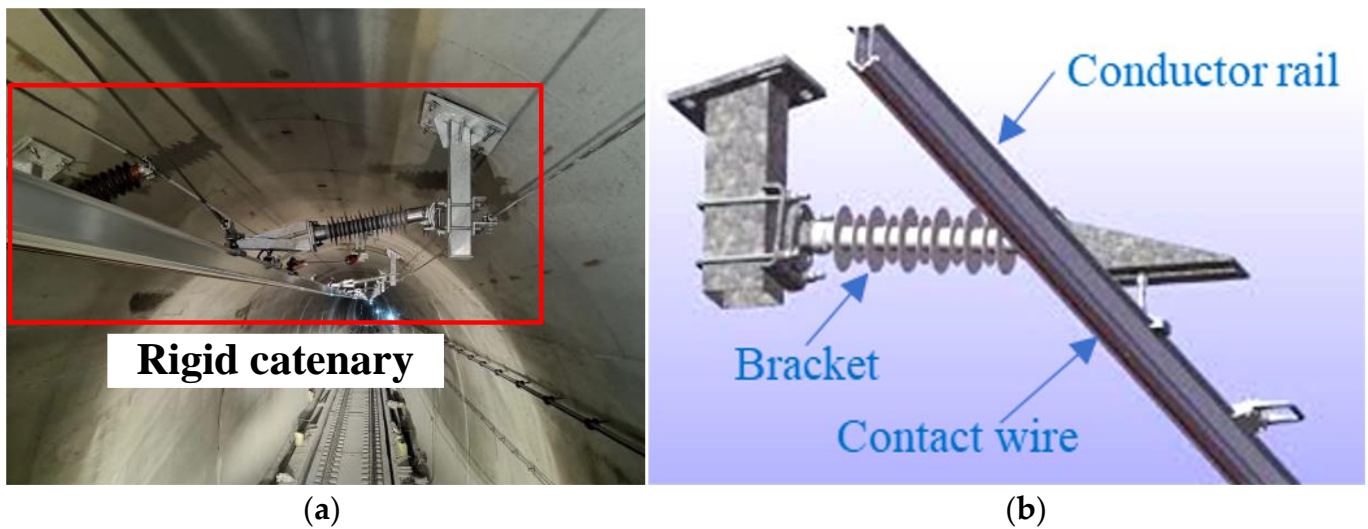
Figure 1. Schematics of a rigid catenary system. (**a**) presents an overall rigid catenary; (**b**) illustrates the main components of a rigid catenary system.

1.1. Problem Description

The contact quality between the contact wire of the catenary and the pantograph collector mainly determines the quality of the electric transformation to the train. For traditional soft catenary, the main factor limiting train speed is the wave speed, which is determined by the tension in the catenary [3]. This issue is overcome by the rigid catenary, which has a much faster wave speed. However, the biggest issue for rigid catenary is the geometry of the contact wire. When the stiffness increases, the irregularity and the sag in the contact wire have a more noticeable effect on the interaction performance with a pantograph. Due to gravity, the contact wire of the rigid catenary is not completely horizontal, and a certain amount of sag is presented, which may have a negative effect on the interaction performance with a pantograph. That is why the operating speed for most rigid catenary systems is limited to lower than 160 km/h [4]. The smoothness of the contact wire needs to be improved to satisfy a higher-speed operation requirement. When constructing a rigid catenary, it is theoretically possible to reduce the sag by reducing the span length, which often results in the roar of the economic cost. Therefore, it is very promising to reduce the contact wire sag by changing the inherent properties of the conductor rail itself. Therefore, a new type of conductor rail with a large moment of inertia should be developed, and its performance deserves to be investigated.

1.2. Literature Review

Recently, many scholars have devoted attention and effort to studying pantograph-catenary interaction performance, as it is an essential part of traction power systems [5]. However, most focus on the traditional soft catenary system as it is the main power source for electric trains. The finite element approach is the most popular method to represent the mechanical behaviors of catenary systems [6,7]. The pantograph is often assumed to be a lumped mass [8] or a multibody model [9,10]. Several approaches [11,12] have been developed to co-simulate the pantograph and the catenary system. To accurately reproduce the pantograph-catenary behavior, hardware-in-the-loop tests comprised of a realistic pantograph and a mimic catenary are developed [13,14]. To ensure numerical accuracy, the measured response of the pantograph-catenary from field tests is used to validate numerical models [15]. Due to the complex working environment of the railway system [16,17], various types of disturbances to the pantograph-catenary have been considered in recent studies. The impacts of catenary defects [18–21], contact wire irregularities [22–25], wave disturbances [26–30], vehicle-track perturbations [31–33], pantograph aerodynamics [34–37], and wind load [38–41] in harsh working environments are properly

modeled and involved in the numerical simulation of the pantograph-catenary interaction to quantify their effects on the contact quality.

Regarding the rigid catenary, only a few works have been carried out. As the rigid catenary has a similar geometry to the traditional soft one, some methods already used for studying the soft catenary can be introduced to study the rigid catenary. For example, the finite element approach is also the most popular one to model the rigid catenary. In [42], a finite element model of the rigid catenary is developed based on commercial software. This work also indicates that the cross-sectional area's horizontal moment directly affects contact quality. Using beam elements, a rigid catenary model is developed, and the numerical simulation with a pantograph model is carried out [43]. Unlike the soft catenary, the rigid one is stiffer and has a relatively greater bending stiffness. The contact wire irregularity presents the main source of deterioration of the interaction performance for the rigid catenary-pantograph system. The distant effect of the irregularity on the contact quality has been acknowledged in [44]. For rigid catenary, Shimizu et al. [45] studied the evolvement of the wear on T-type conductor rail. They discovered that the contact loss and wear rates significantly increase with undulating wear. Apart from the wear, the geometry distortion also has an important effect on the contact quality, as demonstrated in [20]. For the rigid catenary, the most significant geometry distortion is the sag of the contact wire caused by gravity. But no measures have been taken to reduce the sag for a better interaction performance of the rigid catenary-pantograph system.

1.3. Contribution of This Paper

The above literature review points out the need to reduce the contact wire sag to improve the interaction performance of the rigid catenary-pantograph. However, no studies have been done to tackle this issue before. The reduction of span length is not always feasible due to the considerable increase in economic cost. Based on a conventional conductor rail, this paper develops six new types of conductor rail with large moment of inertia. Both the static and dynamic analyses are conducted to investigate the performance of these new types of conductor rail with big moments of inertia. Using the 3D solid element, a model of the conductor rail is built. The vertical deflection and the stress distribution are comparatively analyzed among different types of conductor rail. Introducing a pantograph model, the dynamic behavior of the rigid catenary-pantograph is analyzed to check the potential of using a conductor rail with a large moment of inertia to improve dynamic performance.

2. Modelling of Conductor Rail Model

2.1. Description of Conductor Rail Model

Rigid catenary conductor rail generally has two types, π-type and T-type. At present, the π-type conductor rail model is mainly used in China. This paper focuses on the existing common one and proposes six new types of large moment of inertia for better performance. The π-shaped conductor rail is extruded from 6101B-T6. As shown in Figure 2, there is a clamp at the bottom, which can be elastically opened to embed the contact wire, and the pressure generated by elasticity clamps the contact wire. The rigid catenary system is modeled in the commercial finite element software Ansys, in which a detailed conductor rail is modeled with 3D solid elements. Figure 2 presents a conventional cross-sectional shape of the conductor rail and the contact wire.
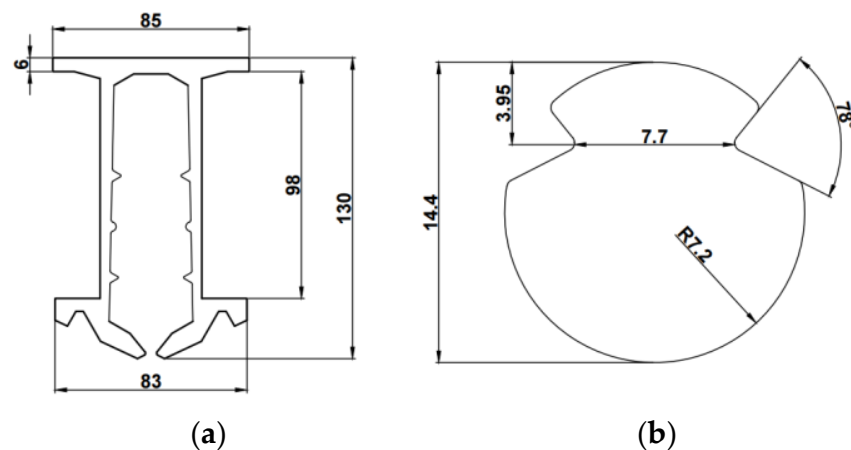
Figure 2. Schematics of conductor rail (**a**) and contact wire (**b**).

In Solidworks, the conductor rail and contact wire are modeled according to their realistic geometry (Figure 3). The total length is modeled as 12,000 mm with a span length of 8 m. The material properties, including the conductor rail's density and elastic modulus, are set to aluminum alloy. According to EN AW 6101B, aluminum accounts for more than 95%, and the material properties are mainly affected by aluminum. The density is 2.7 g/cm^3, and the elastic modulus is 72 Gpa. The contact wire material is set to copper alloy. The density is 8.9 g/cm^3, and the modulus of elasticity is 120 Gpa. After loading the model in Anasys, a 4-node planar element, the solid 182 unit is used to mesh the rigid catenary, as shown in Figure 4a. The grid at the conductor rail is evenly divided. The mesh of the contact wire and the connection surface between the contact wire and the clamp is finer to ensure numerical accuracy. For the case of analysis, the total number of elements used to mesh the conductor rail is 1379, and the number of nodes is 1672; the number of 110-height busbar units is 1289, and the number of nodes is 1564. The constraints are applied as demonstrated in Figure 4b, in which the support is added at an interval of 8 m.
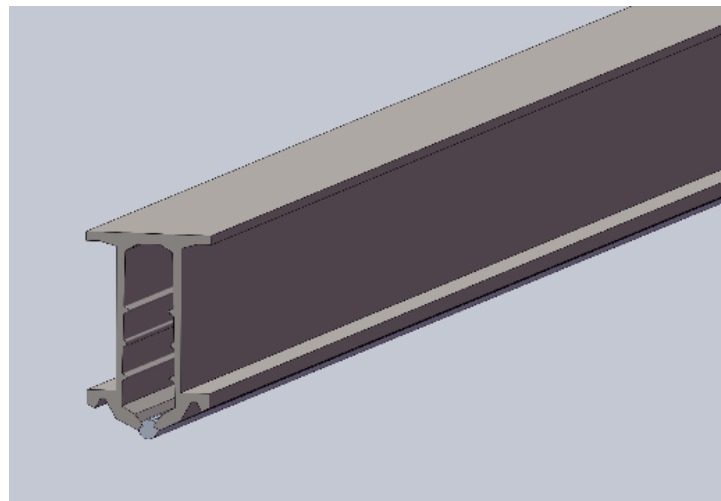

Figure 3. Conductor rail and contact wire model in Solidworks.

(**a**)

(**b**)
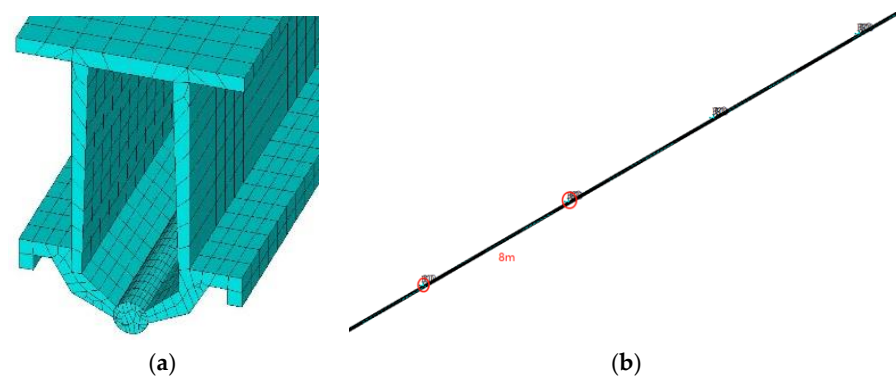
Figure 4. Finite element model of rigid catenary. (**a**) Presents a local view of the mesh on the cross-section; (**b**) Presents a global view to show the constraint of each support.

In actual operation, the sag of the conductor rail caused by gravity directly impacts the static and dynamic characteristics of the rigid catenary-pantograph interaction. In the construction phase, it is theoretically possible to reduce the sag by reducing the span, though this may increase the economic cost. Therefore, reducing the rigid network sag by changing the inherent properties of the conductor rail itself is very promising. Under the premise of the requirement of the standard, a total of 6 new types of conductor rail are designed here, referred to as "large moment of inertia conductor rails", as shown in Figure 5. Compared with the conventional conductor rails, the large moment of inertia increases the vertical height, thereby increasing the sheer moment of inertia, which has a better capability to resist vertical bending. It should be noted that the increase in vertical height may result in marginally lowering the pantograph or increasing the tunnel cost. The latter measure may offset the reduction in rigid conductor rail cost and deserves a further trade-off study. The subsequent analysis will investigate the performance of these six new types under static and dynamic load through three-dimensional finite element analysis.
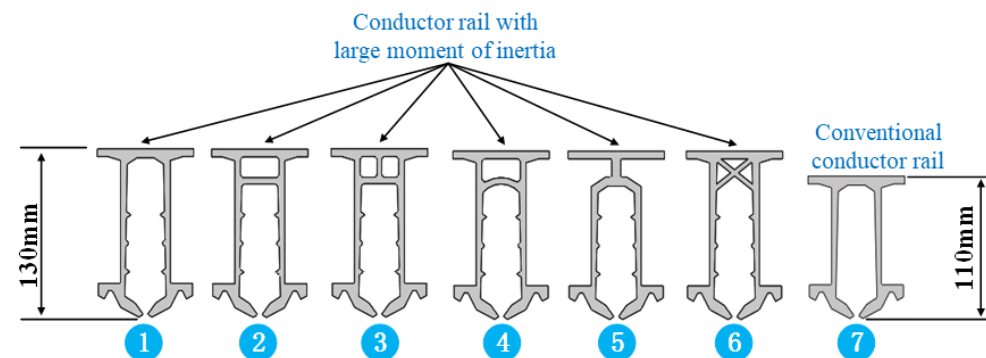
Figure 5. Six new types of conductor rail with large moment of inertia denoted as No. 1–6, and the conventional one denoted as No. 7.

2.2. Finite Element Model of Conductor Rail Model

In this paper, the Timoshenko beam element is mainly adopted to model the conductor rail and contact wire. The stiffness element matrix of the Timoshenko beam element is written as Equation (1).

$$
K_b = \begin{bmatrix}
\frac{EA}{l} & 0 & 0 & 0 & 0 & 0 & \frac{-EA}{l} & 0 & 0 & 0 & 0 & 0 \\
0 & \frac{12EI_z}{l^3(1+\phi_y)} & 0 & 0 & 0 & \frac{6EI_z}{l^2(1+\phi_y)} & 0 & \frac{-12EI_z}{l^3(1+\phi_y)} & 0 & 0 & 0 & \frac{6EI_z}{l^2(1+\phi_y)} \\
0 & 0 & \frac{12EI_y}{l^3(1+\phi_z)} & 0 & \frac{-6EI_y}{l^2(1+\phi_z)} & 0 & 0 & 0 & \frac{-12EI_y}{l^3(1+\phi_z)} & 0 & \frac{-6EI_y}{l^2(1+\phi_z)} & 0 \\
0 & 0 & 0 & \frac{GJ}{l} & 0 & 0 & 0 & 0 & 0 & \frac{-GJ}{l} & 0 & 0 \\
0 & 0 & \frac{-6EI_y}{l^2(1+\phi_z)} & 0 & \frac{(4+\phi_z)EI_y}{l(1+\phi_z)} & 0 & 0 & 0 & \frac{-GJ}{l} & 0 & \frac{(2-\phi_z)EI_y}{l(1+\phi_z)} & 0 \\
0 & \frac{6EI_z}{l^2(1+\phi_y)} & 0 & 0 & 0 & \frac{(4+\phi_y)EI_z}{l(1+\phi_y)} & 0 & \frac{-6EI_z}{l^2(1+\phi_y)} & 0 & 0 & 0 & \frac{(2-\phi_y)EI_z}{l(1+\phi_y)} \\
\frac{-EA}{l} & 0 & 0 & 0 & 0 & 0 & \frac{AE}{l} & 0 & 0 & 0 & 0 & 0 \\
0 & \frac{-12EI_z}{l^3(1+\phi_y)} & 0 & 0 & 0 & \frac{-6EI_z}{l^2(1+\phi_y)} & 0 & \frac{12EI_z}{l^3(1+\phi_y)} & 0 & 0 & 0 & \frac{-6EI_z}{l^2(1+\phi_y)} \\
0 & 0 & \frac{-12EI_y}{l^3(1+\phi_z)} & 0 & \frac{6EI_y}{l^2(1+\phi_z)} & 0 & 0 & 0 & \frac{12EI_y}{l^3(1+\phi_z)} & 0 & \frac{6EI_y}{l^2(1+\phi_z)} & 0 \\
0 & 0 & 0 & \frac{-GJ}{l} & 0 & 0 & 0 & 0 & 0 & \frac{GJ}{l} & 0 & 0 \\
0 & 0 & \frac{-6EI_y}{l^2(1+\phi_z)} & 0 & \frac{(2-\phi_z)EI_y}{l(1+\phi_z)} & 0 & 0 & 0 & \frac{6EI_y}{l^2(1+\phi_z)} & 0 & \frac{(4+\phi_z)EI_y}{l(1+\phi_z)} & 0 \\
0 & \frac{6EI_z}{l^2(1+\phi_y)} & 0 & 0 & 0 & \frac{(2-\phi_y)EI_z}{l(1+\phi_y)} & 0 & \frac{-6EI_z}{l^2(1+\phi_y)} & 0 & 0 & 0 & \frac{(4+\phi_y)EI_z}{l(1+\phi_y)}
\end{bmatrix} \tag{1}
$$

where E is elastic modulus, A is area of section, I_y is moment of inertia in y direction, I_z is the moment of inertia in z direction, l is the length of the beam, $\phi_y = \frac{12EI_z}{GA_yl^2}$ (A_y is the shear area in the y direction), $\phi_z = \frac{12EI_y}{GA_zl^2}$ (A_z is the shear area in the z direction), G is shear modulus.

The whole suspension structure is adopted by the spring-damper element and the lumped mass element. The spring-damper element has longitudinal or torsional capability in 1-D, 2-D, or 3-D applications, and the lumped mass element has six degrees of freedom. The element matrix is written as Equations (2) and (3).

$$
K_e = k \begin{bmatrix} 1 & -1 \\ -1 & 1 \end{bmatrix}, C_e = C_v \begin{bmatrix} 1 & -1 \\ -1 & 1 \end{bmatrix} \tag{2}
$$

where k is stiffness, C_v is damping coefficient, obtained from $C_v = C_{v1} + C_{v2}$, C_{v1} is constant damping coefficient, C_{v2} is linear damping coefficient, v is relative velocity.

$$
M_e = \begin{bmatrix}
a & 0 & 0 & 0 & 0 & 0 \\
0 & b & 0 & 0 & 0 & 0 \\
0 & 0 & c & 0 & 0 & 0 \\
0 & 0 & 0 & d & 0 & 0 \\
0 & 0 & 0 & 0 & f & 0 \\
0 & 0 & 0 & 0 & 0 & g
\end{bmatrix} \tag{3}
$$

where a, b, c, d, e, f is used for masses and moment of inertia.

The equation of rigid catenary can be described as follows based on FEM.

$$
M_c \ddot{U}_c + C_c \dot{U}_c + K_c U_c = G_c + F_c \tag{4}
$$

where M_c and K_c are the mass matrix and stiffness matrix. C_c is the Rayleigh damping matrix, a combination of mass matrix and stiffness matrix. U_c is the displacement vector of the rigid catenary. G_c is the gravity matrix, and F_c is the contact force matrix.

3. Static Analysis

This section investigates the deflection and clamping stress of these new types of conductor rail with realistic constraints and gravity. According to the Chinese industrial standard for overhead conductor rail, TB/T 3252 [46], the deflection of the conductor rail should be checked with a specified length of 12 m, which is conducted in Section 3.1. Then the deflection of conductor rail with multi-spans under realistic constraints and gravity is analyzed in Section 3.2. Finally, the clamping stress with a contact wire in realistic working conditions is investigated.

3.1. Analysis of Deflection with the Standard Specification

TB/T 3252 stipulates that the maximum sag allowance of the simply supported conductor rail with a length of 12 m should be ≤70 mm. In this section, the models of conductor rail for six new types and the conventional one with a single span are built. After applying gravity, the static deflection can be extracted, as demonstrated in Figure 6. It can be seen from Figure 6 that the sag of the conductor rail with a large moment of inertia is greatly reduced compared with the conventional one. To facilitate the comparison, Table 1 collects the resulting maximum deflection of all cases. It is observed that the sag of the conventional conductor rail is the largest, which is 67.519 mm. After the conductor rail with a large conductor rail is used, the maximum sag is significantly reduced. The best performance can be observed in case 1, in which the maximum sag only reaches 48.58 mm, while the others are generally at the same level of around 50 mm.

Table 1. Maximum sag of the conductor rail with standard specification.

Type	Maximum [mm]
Conductor rail 1	48.580
Conductor rail 2	50.865
Conductor rail 3	50.831
Conductor rail 4	50.990
Conductor rail 5	51.398
Conductor rail 6	50.323
Conductor rail 7	67.519

3.2. Analysis of Deflection with Multi Spans

This section uses a multi-span model of conductor rail with a span length of 8 m to check the conductor rail deflection under realistic conditions. The diagrams of the resulting deflection are presented in Figure 7. Each span has a similar deflection shape due to the periodicity, but the sags in the side spans are higher due to the boundary constraint effect. Normally, only the central spans are taken as the analysis object to avoid the effect from the boundary effect [47]. It is seen in Figure 7 that the sags of the conductor rails with large moments of inertia are smaller than the conventional ones. Table 2 collects the resulting maximum deflection of all cases. The sag of the conventional conductor rail is the largest at 2.7120 mm. After the conductor rail with a large conductor rail is used, the maximum sag is significantly reduced. The best performance can be observed in case 1, where the maximum sag is reduced to 1.9426 mm by 28.37% compared with the conventional conductor. For others, the mid-span sags are generally reduced to around 2 mm.
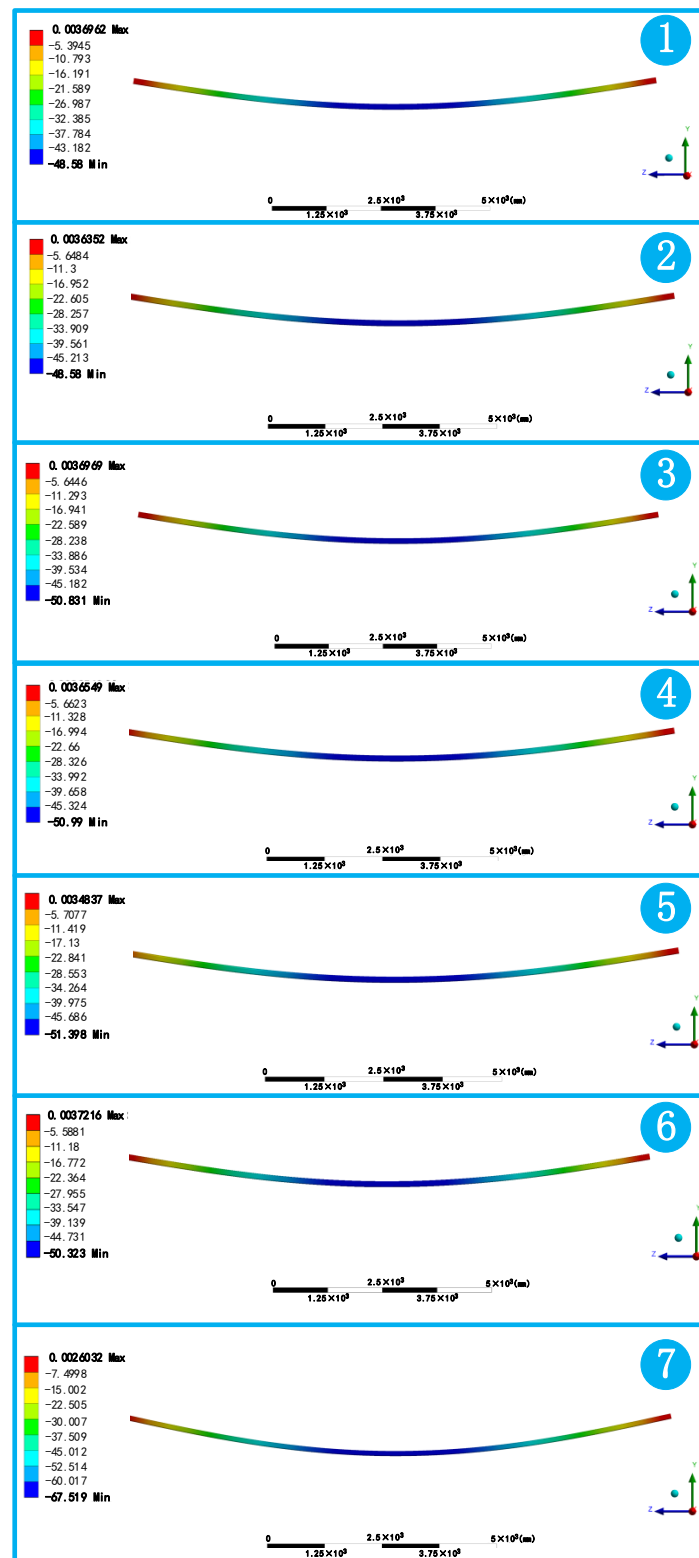
Figure 6. Static deflections of conductor rail with standard specification. No. 1–6 denote the results of new types of conductor rail with large moment of inertia, and the result of the conventional one is denoted as No. 7.

Figure 7. Static deflections of multi-span conductor rail. No. 1–6 denote the results of new types of conductor rail with large moment of inertia, and the result of the conventional one is denoted as No. 7.
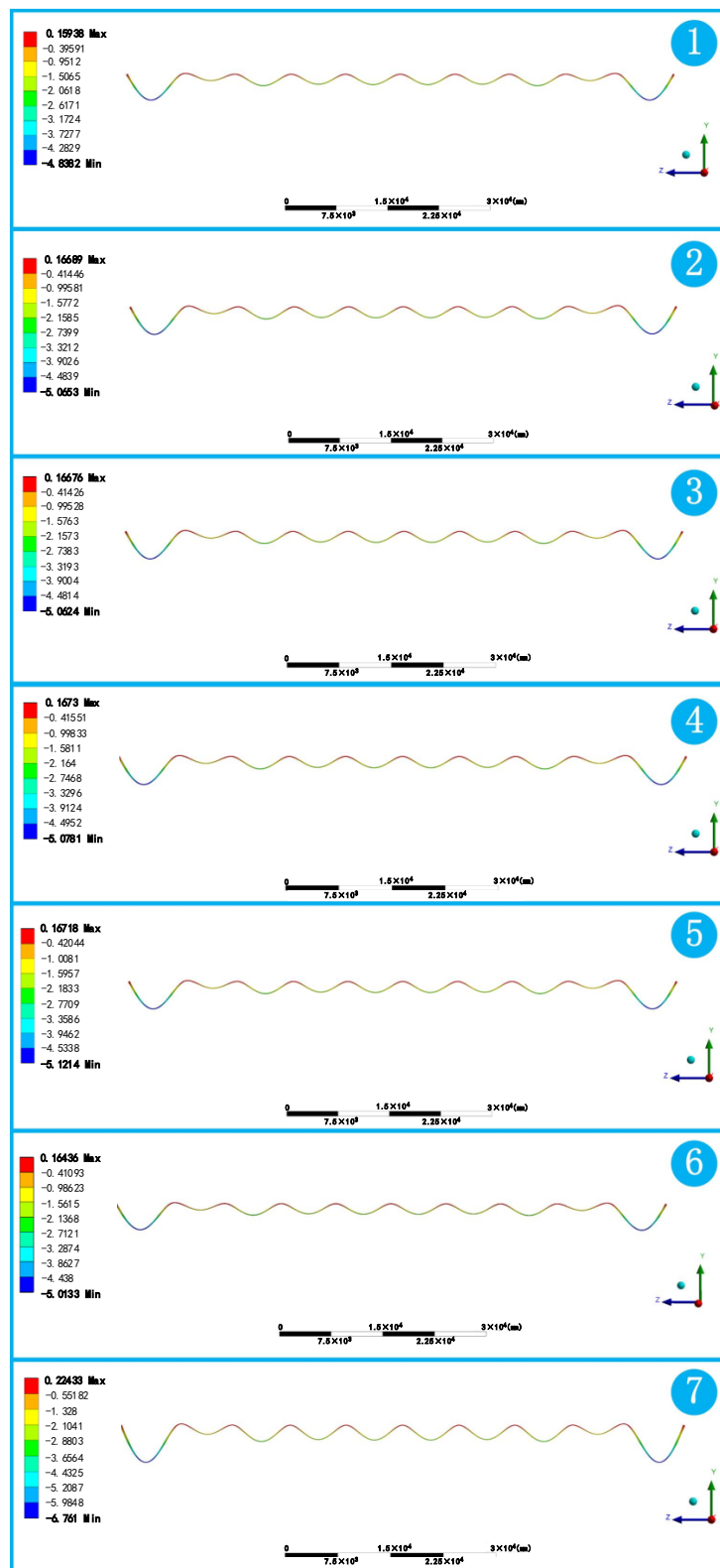
Table 2. Maximum sag of the multi-span conductor rail.

Type	Maximum [mm]
Conductor rail 1	1.9426
Conductor rail 2	2.0339
Conductor rail 3	2.0325
Conductor rail 4	2.0391
Conductor rail 5	2.0574
Conductor rail 6	2.0142
Conductor rail 7	2.7120

3.3. Analysis of Clamp Stress

According to TB/T 3252, the jaw on the conductor rail should be open to 2.5 mm to represent the presence of the contact wire and check the clamping stress. In this work, the horizontal load is applied to the jaws of the two dovetail grooves of the conductor rail in a uniform distribution to ensure that each side of the jaw opens 2.5 mm. The setting process is shown in Figure 8. The diagrams of the resulting stress distribution are presented in Figure 9. It is seen that the maximum stress appears on the side surface of the conductor rail. To facilitate the comparison, Table 3 collects the maximum stress and the maximum clamping force in the conductor rail. It is observed that the maximum clamping force and the stress of the No. 1 conductor rail are the largest among all cases, which reaches 4560 N and 80.92 Mpa, respectively. After the conductor rail with a large moment of inertia is used, the clamping force is significantly reduced. However, regarding the maximum stress, not all the new types of conductor rail with large moments of inertia perform better than the conventional one. Only the first one exhibits a significant reduction in the maximum stress from 112.02 Mpa to 80.92 Mpa by 27.76%.

A: Right of the jaw
B: Right of the jaw

Each side of the jaw opens 2.5mm

Horizontal load
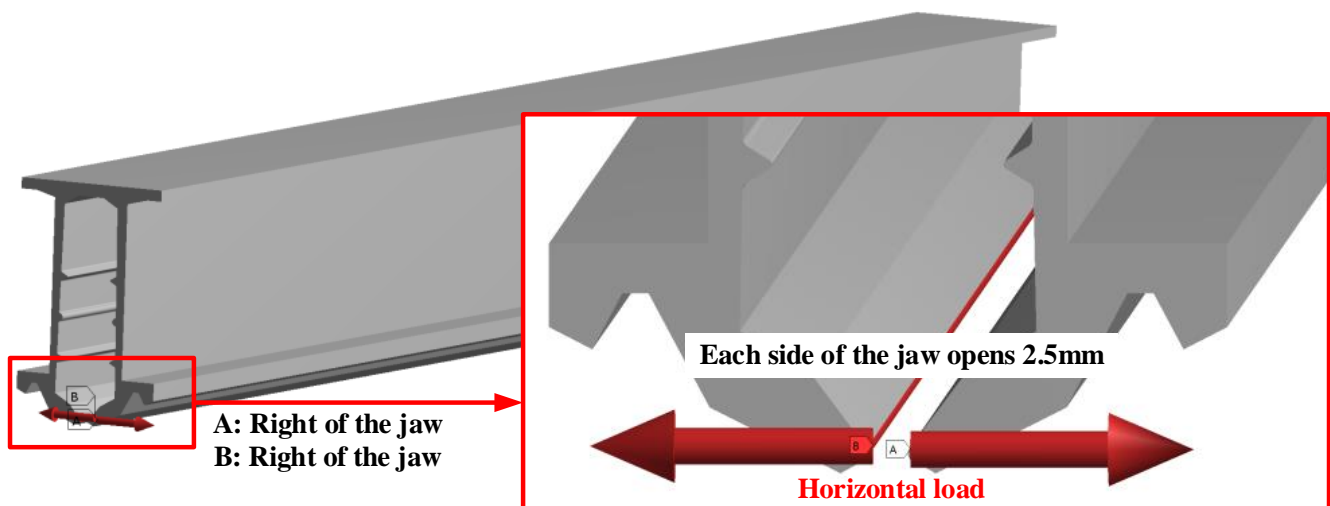
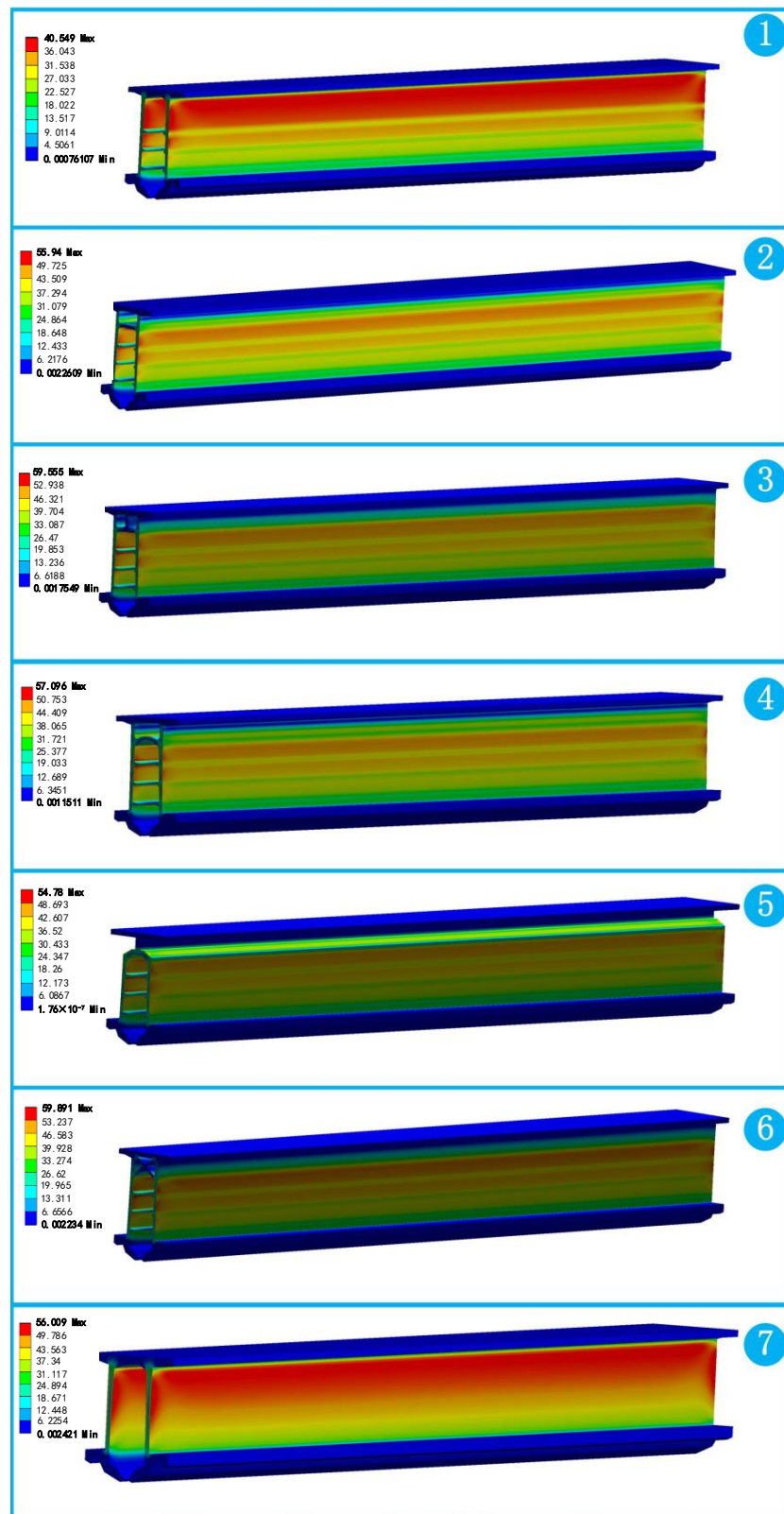**Figure 8.** Schematics of applying clamping loads.

Figure 9. Stress distribution on conductor rail. No. 1–6 denote the results of new types of conductor rail with large moment of inertia, and the result of the conventional one is denoted as No. 7.

**Table 3.** Maximum clamping force and stress of conductor rails.

Type	Maximum Clamping Force [N]	Maximum Stress [MPa]
Conductor rail 1	4560	80.920
Conductor rail 2	6780	111.88
Conductor rail 3	7080	119.11
Conductor rail 4	6840	114.19
Conductor rail 5	6380	109.56
Conductor rail 6	7260	119.78
Conductor rail 7	7600	112.02

4. Dynamic Analysis

In this section, a pantograph framework model is included to check the dynamic performance of the rigid catenary with different types of conductor rail. Considering the considerable computational cost of the 3D solid finite element model, the conductor rail and the contact wire are simplified to Timoshenko beam elements in the dynamic simulation. Some essential parameters of the beam element, including the cross-sectional area and the moment of inertia, are determined by the solid model of the rigid catenary, as described above. The key parameters of rigid catenary are collected in Table 4. The pantograph-rigid catenary dynamic model is visualized in Figure 10. Here the pantograph is modeled as a lumped mass representation as described in [48]. The parameters of the DSA250 pantograph are shown in Table 5. The dynamic simulation is performed at 160 km/h and 200 km/h. The former is the maximum speed for most commercial lines using rigid catenary systems worldwide, while the latter is the target of speed upgrade for the next generation of the rigid catenary system.

**Table 4.** Key parameters of rigid catenary.

| Quantity	Value	Unit
Moment of inertia of conductor rail	5.7277×10^{-6}	m^4
The density of conductor rail	2700	Kg/m^3
Conductor rail Yough's modulus	72	Gpa
Contact wire density	8900	Kg/m^3
Contact wire Yough's modulus	120	Gpa
Number of spans	30	-
Span length	8	m
Support stiffness	6.7×10^7	N/m
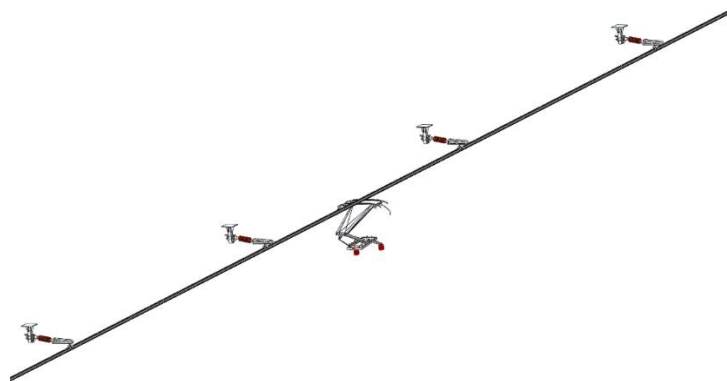
Figure 10. Visualized pantograph-rigid catenary model used in dynamic simulation.

Table 5. Parameters of DSA250 pantograph.

Parameter	Value	Unit
m1	7.51	Kg
m2	5.855	Kg
m3	4.645	Kg
k1	8380	N/m
k2	6200	N/m
k3	80	N/m
c1	0	Ns/m
c2	0	Ns/m
c3	70	Ns/m

According to the European standard En 50367 [3], the contact force between the pantograph and the catenary is the most direct reflection of the contact quality. Normally, the contact force is expected to be stable without a big fluctuation. Therefore, contact force statistics are often used to evaluate interaction performance. The contact force standard deviation is expected to be decreased to reduce the fluctuation in contact force. Reduction of the maximum contact force is desired, while the minimum contact force is expected to increase. Figure 11a,b present the contact force standard deviation, maximum contact force, and minimum contact force, respectively. The total length of the conductor rail is 240 m, and the contact forces collected from the central 150 m are taken in the statistical analysis. It is seen from Figure 11a that the conventional conductor rail (with case 7) leads to the biggest contact force standard deviation among all cases. The standard deviation is significantly reduced when the conductor rail with a large moment of inertia is used. Figure 11b demonstrates that the conventional conductor rail leads to the biggest maximum contact force. The maximum contact force is reduced using the developed conductor rail with a large moment of inertia, resulting in safer operation. Figure 11c shows that the minimum contact force experiences a significant increase when the developed conductor rails with large moments of inertia are used. Generally, the conductor rails of cases 1 and 6 show the best performance in terms of the contact force standard deviation and the minimum contact force. The contact force standard deviations are reduced by over 32% and 27% at 160 km/h and 200 km/h, respectively, while the minimum contact forces are reduced by over 14% and 24% at these two speeds. As for the maximum contact force, the conductor rail of case 1 shows better performance than case 6. In case 1, the maximum contact forces are reduced by 4.43% and 5.8% at 160 km/h and 200 km/h, respectively. Therefore, the conductor rail of case 1 generally shows the best performance in improving the interaction performance of the pantograph-rigid catenary.

(a)

Figure 11. *Cont.*

(b)

(c)
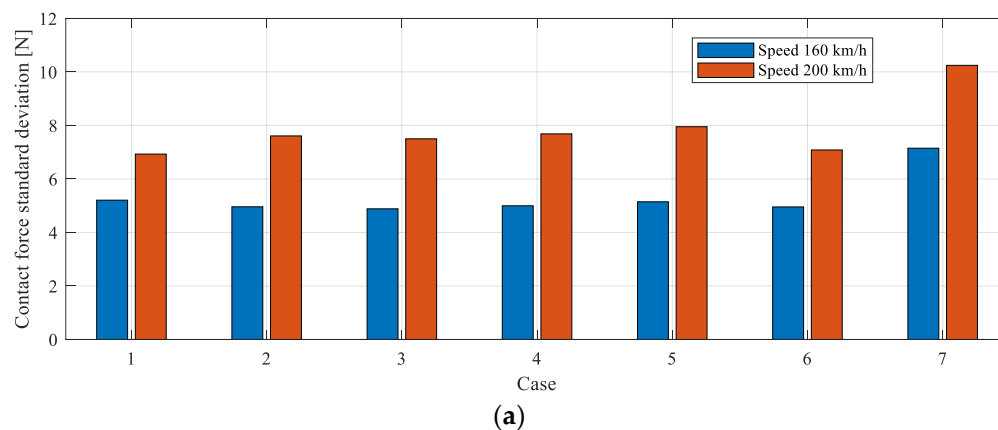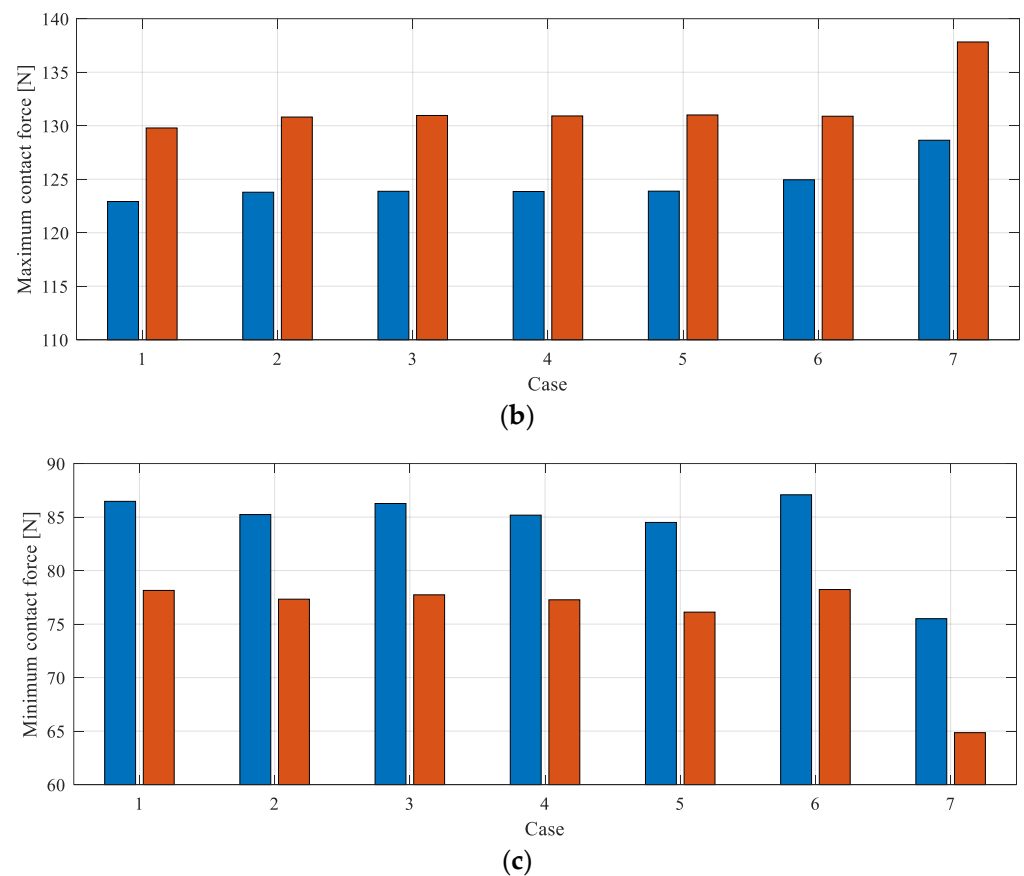
Figure 11. Contact force statistics with different types of conductor rail. (**a**) Presents the resulting contact force standard deviation; (**b**) The resulting maximum contact force; (**c**) The resulting minimum contact force. Cases 1–6 represent the results with conductor rails of large moment of inertia, and Case 7 denotes the result with the previous conventional conductor rail.

5. Conclusions

The main contributions and conclusions in this work have been listed as follows:

(1)   To improve both the static and dynamic performance of the rigid catenary system, six new types of conductor rail with large moment of inertia are developed in this paper. The comparative analysis indicates that the vertical deflection and stress distribution are significantly improved when using the conductor rail with a large moment of inertia.

(2)   Regarding the deflection assessment with the standard specification, cases 1–6 can generally reduce the maximum sag from 67.519 mm, close to the safety threshold of around 50 mm. Among these cases, the best performance is observed in Case 1. Case 1 also outperforms the assessment of stress and dynamic behavior. Compared with other cases, the conductor rail with case 1 can provide a bigger moment of inertia with the specific cross-sectional height. In case 1, the maximum sag is reduced by 28.37% compared with the conventional conductor, while the maximum stress is decreased by 27.76%.

(3)   The contact force fluctuation is significantly reduced after using the conductor rails with large moments of inertia. The conductor rail of case 1 shows the best performance in improving the dynamic interaction performance.

This study has numerically demonstrated the potential value of improving the moment of inertia for conductor rails of rigid catenary. The next step is implementing the developed conductor rail with a large moment of inertia in a field test to further validate the current collection quality and service safety. This conductor rail with a big moment of inertia

may be a potential solution for the high-speed rigid catenary system in mountainous areas. Another issue this work separately assesses is the static and dynamic performance of the conductor rail. A comprehensive indicator may be preferred to be developed in future works.

References

1. Chen, J.; Yang, T.; Zhang, D.; Huang, H.; Frontiers, Y.-G. *Deep Learning Based Classification of Rock Structure of Tunnel Face*; Elsevier: Amsterdam, The Netherlands, 2021. Available online: https://www.sciencedirect.com/science/article/pii/S1674987120300931 (accessed on 1 February 2023).
2. Chen, J.; Zhou, M.; Huang, H.; Zhang, D.; Rock, Z.-I. *Automated Extraction and Evaluation of Fracture Trace Maps from Rock Tunnel face Images via Deep Learning*; Elsevier: Amsterdam, The Netherlands, 2021. Available online: https://www.sciencedirect.com/science/article/pii/S1365160921001313 (accessed on 1 February 2023).
3. *EN 50367*; Railway Applications—Current Collection Systems—Technical Criteria for the Interaction between Pantograph and Overhead Line. European Standards (EN): Brussels, Belgium, 2016.
4. Dai, H. Research on 200 km/h AC Rigid Catenary Scheme. 2019. Available online: https://d.wanfangdata.com.cn/thesis/ChJUaGVzaXNOZXdTMjAyMzAxMTISCUQwMTg1OTE3MRoIa3c2cGluN2w%3D (accessed on 1 February 2023).
5. Chen, H.; Jiang, B. A Review of Fault Detection and Diagnosis for the Traction System in High-Speed Trains. *IEEE Trans. Intell. Transp. Syst.* **2021**, *21*, 450–465. [CrossRef]
6. Bruni, S.; Ambrosio, J.; Carnicero, A.; Cho, Y.; Finner, L.; Ikeda, M.; Kwon, S.; Massat, J.; Stichel, S.; Tur, M.; et al. The results of the pantograph-catenary interaction benchmark. *Veh. Syst. Dyn.* **2015**, *53*, 412–435. [CrossRef]
7. Song, Y.; Rønnquist, A.; Jiang, T.; Nåvik, P. Railway pantograph-catenary interaction performance in an overlap section: Modelling, validation and analysis. *J. Sound Vib.* **2023**, *548*, 117506. [CrossRef]
8. Song, Y.; Liu, Z.; Ouyang, H.; Wang, H.; Lu, X. Sliding Mode Control with PD Sliding Surface for High-Speed Railway Pantograph-Catenary Contact Force under Strong Stochastic Wind Field. *Shock. Vib.* **2017**, *2017*, 4895321. [CrossRef]
9. Song, Y.; Ouyang, H.; Liu, Z.; Mei, G.; Wang, H.; Lu, X. Active control of contact force for high-speed railway pantograph-catenary based on multi-body pantograph model. *Mech. Mach. Theory* **2017**, *115*, 35–59. [CrossRef]
10. Pombo, J.; Ambrósio, J.; Pereira, M. Influence of pantograph components on the contact quality of the overhead system for high speed trains. *Civ.-Comp. Proc.* **2010**, *93*. [CrossRef]
11. Jimenez-Octavio, J.; Carnicero, A.; Sanchez-Rebollo, C.; Such, M. A moving mesh method to deal with cable structures subjected to moving loads and its application to the catenary-pantograph dynamic interaction. *J. Sound Vib.* **2015**, *349*, 216–229. [CrossRef]
12. Ambrósio, J.; Pombo, J.; Rauter, F.; Pereira, M. A Memory Based Communication in the Co-simulation of Multibody and Finite Element Codes for Pantograph-Catenary Interaction Simulation. In *Multibody Dynamics*; Springer: Dordrecht, The Netherlands, 2009; pp. 231–252. [CrossRef]
13. Kobayashi, S.; Stoten, D.; Yamashita, Y.; Usuda, T. Dynamically substructured testing of railway pantograph/catenary systems. *Proc. Inst. Mech. Eng. F. J. Rail. Rapid. Transit.* **2019**, *233*, 516–525. [CrossRef]
14. Bruni, S.; Bucca, G.; Collina, A.; Facchinetti, A. Numerical and hardware-in-the-loop tools for the design of very high speed pantograph-catenary systems. *J. Comput. Nonlinear Dyn.* **2012**, *7*, 041013. [CrossRef]
15. Nåvik, P.; Rønnquist, A.; Stichel, S. Variation in predicting pantograph–catenary interaction contact forces, numerical simulations and field measurements. *Veh. Syst. Dyn.* **2017**, *55*, 1265–1282. [CrossRef]
16. Zhang, L.; Wang, Z.; Wang, Q.; Mo, J.; Feng, J.; Wang, K. The effect of wheel polygonal wear on temperature and vibration characteristics of a high-speed train braking system. *Mech. Syst. Signal. Process* **2023**, *86*, 109864. [CrossRef]
17. Ye, Y.; Zhu, B.; Huang, P.; Peng, B. OORNet: A deep learning model for on-board condition monitoring and fault diagnosis of out-of-round wheels of high-speed trains. *Measurement* **2022**, *199*, 111268. [CrossRef]
18. Vesali, F.; Rezvani, M.; Molatefi, H.; Hecht, M. Static form-finding of normal and defective catenaries based on the analytical exact solution of the tensile Euler–Bernoulli beam. *Proc. Inst. Mech. Eng. F. J. Rail. Rapid. Transit.* **2019**, *233*, 691–700. [CrossRef]

19. Song, Y.; Liu, Z.; Lu, X. Dynamic Performance of High-Speed Railway Overhead Contact Line Interacting With Pantograph Considering Local Dropper Defect. *IEEE Trans. Veh. Technol.* **2020**, *69*, 5958–5967. [CrossRef]

20. Song, Y.; Jiang, T.; Nåvik, P.; Rønnquist, A. Geometry deviation effects of railway catenaries on pantograph–catenary interaction: A case study in Norwegian Railway System. *Railw. Eng. Sci.* **2021**, *29*, 350–361. [CrossRef]

21. Song, Y.; Wang, H.; Liu, Z. An Investigation on the Current Collection Quality of Railway Pantograph-Catenary Systems with Contact Wire Wear Degradations. *IEEE Trans. Instrum. Meas.* **2021**, *70*, 1–11. [CrossRef]

22. Song, Y.; Liu, Z.; Rxnnquist, A.; Navik, P.; Liu, Z. Contact Wire Irregularity Stochastics and Effect on High-speed Railway Pantograph-Catenary Interactions. *IEEE Trans. Instrum. Meas.* **2020**, *69*, 8196–8206. [CrossRef]

23. Song, Y.; Rønnquist, A.; Jiang, T.; Nåvik, P. Identification of short-wavelength contact wire irregularities in electrified railway pantograph–catenary system. *Mech. Mach. Theory* **2021**, *162*, 104338. [CrossRef]

24. Qin, Y.; Zhang, Y.; Cheng, X.; Jia, L.; Xing, Z. An analysis method for correlation between catenary irregularities and pantograph-catenary contact force. *J. Cent. South Univ.* **2014**, *21*, 3353–3360. [CrossRef]

25. Song, Y.; Antunes, P.; Pombo, J.; Liu, Z. A methodology to study high-speed pantograph-catenary interaction with realistic contact wire irregularities. *Mech. Mach. Theory* **2020**, *152*, 103940. [CrossRef]

26. Xu, Z.; Song, Y.; Liu, Z. Effective Measures to Improve Current Collection Quality for Double Pantographs and Catenary Based on Wave Propagation Analysis. *IEEE Trans. Veh. Technol.* **2020**, *69*, 6299–6309. [CrossRef]

27. Song, Y.; Liu, Z.; Duan, F.; Xu, Z.; Lu, X. Wave propagation analysis in high-speed railway catenary system subjected to a moving pantograph. *Appl. Math. Model.* **2018**, *59*, 20–38. [CrossRef]

28. Song, Y.; Duan, F.; Liu, Z. Analysis of Critical Speed for High-Speed Railway Pantograph-Catenary System. *IEEE Trans. Veh. Technol.* **2022**, *71*, 3547–3555. [CrossRef]

29. Van, O.V.; Massat, J.; Balmes, E. Waves, modes and properties with a major impact on dynamic pantograph-catenary interaction. *J. Sound Vib.* **2017**, *402*, 51–69. [CrossRef]

30. Vesali, F.; Rezvani, M.; Molatefi, H. Analysis of conceptual similarities and differences of wave speed and critical speed in the overhead catenary system. *Measurement* **2021**, *176*, 109164. [CrossRef]

31. Pombo, J.; Ambrosio, J. Environmental and track perturbations on multiple pantograph interaction with catenaries in high-speed trains. *Comput. Struct.* **2013**, *124*, 88–101. [CrossRef]

32. Carnicero, A.; Jimenez-Octavio, J.; Sanchez-Rebollo, C.; Ramos, A.; Such, M. Influence of track irregularities in the catenary-pantograph dynamic interaction. *J. Comput. Nonlinear Dyn.* **2012**, *7*, 041015. [CrossRef]

33. Song, Y.; Wang, Z.; Liu, Z.; Wang, R. A spatial coupling model to study dynamic performance of pantograph-catenary with vehicle-track excitation. *Mech. Syst. Signal. Process* **2021**, *151*, 107336. [CrossRef]

34. Li, R.; Zhang, W.; Ning, Z.; Liu, B.; Zou, D.; Liu, W. Influence of a high-speed train passing through a tunnel on pantograph aerodynamics and pantograph-catenary interaction. *Proc. Inst. Mech. Eng. F. J. Rail. Rapid Transit.* **2017**, *231*, 198–210. [CrossRef]

35. Shi, H.; Chen, G.; Yang, Y. A comparative study on pantograph-catenary models and effect of parameters on pantograph-catenary dynamics under crosswind. *J. Wind. Eng. Ind. Aerodyn.* **2021**, *211*, 104587. [CrossRef]

36. Carnevale, M.; Facchinetti, A.; Rocchi, D. Procedure to assess the role of railway pantograph components in generating the aerodynamic uplift. *J. Wind. Eng. Ind. Aerodyn.* **2017**, *160*, 16–29. [CrossRef]

37. Li, X.; Zhou, D.; Jia, L.; Yang, M. Effects of yaw angle on the unsteady aerodynamic performance of the pantograph of a high-speed train under crosswind. *J. Wind. Eng. Ind. Aerodyn.* **2018**, *182*, 49–60. [CrossRef]

38. Song, Y.; Zhang, M.; Wang, H. A response spectrum analysis of wind deflection in railway overhead contact lines using pseudo-excitation method. *IEEE Trans. Veh. Technol.* **2021**, *70*, 1169–1178. [CrossRef]

39. Duan, F.; Song, Y.; Gao, S.; Liu, Y.; Chu, W.; Lu, X.; Liu, Z. Study on Aerodynamic Instability and Galloping Response of Rail Overhead Contact Line Based on Wind Tunnel Tests. *IEEE Trans. Veh. Technol.* **2023**. [CrossRef]

40. Song, Y.; Zhang, M.; Øiseth, O.; Rønnquist, A. Wind deflection analysis of railway catenary under crosswind based on nonlinear finite element model and wind tunnel test. *Mech. Mach. Theory* **2022**, *168*, 104608. [CrossRef]

41. Zhang, M.; Xu, F. Tuned mass damper for self-excited vibration control: Optimization involving nonlinear aeroelastic effect. *J. Wind. Eng. Ind. Aerodyn.* **2022**, *220*, 104836. [CrossRef]

42. Vera, C.; Suarez, B.; Paulin, J.; Rodríguez, P. Simulation model for the study of overhead rail current collector systems dynamics, focused on the design of a new conductor rail. *Veh. Syst. Dyn.* **2006**, *44*, 595–614. [CrossRef]

43. Bautista, A.; Montesinos, J.; Pintado, P. Dynamic interaction between pantograph and rigid overhead lines using a coupled FEM—Multibody procedure. *Mech. Mach. Theory* **2016**, *97*, 100–111. [CrossRef]

44. Yamashita, K.; Nakayama, T.; Sugiura, T.; Yabuno, H. Numerical bifurcation analysis of multimode impact oscillations between a pantograph and a rigid conductor line. In Proceedings of the ASME Design Engineering Technical Conference, Chicago, IL, USA, 12–15 August 2012; pp. 955–962. [CrossRef]

45. Shimizu, M.; Harada, S.; Oya, A.; Tokuda, K. Improving performance of type T overhead rigid conductor lines. *Q. Rep. RTRI* **2006**, *47*, 52–58. [CrossRef]

46. *TB/T 3252-2010*; Related Standards. Available online: https://www.chinesestandard.net/Related.aspx/TBT3252-2010 (accessed on 28 December 2022).

47.   *EN 50318*; Railway Applications—Current Collection Systems—Validation of Simulation of the Dynamic Interaction between Pantograph and Overhead Contact Line. European Standards (EN): Brussels, Belgium, 2018.
48.   Chen, L.; Duan, F.; Song, Y.; Hu, Z.; Liu, Z.; Feng, X. Assessment of Dynamic Interaction Performance of High-Speed Pantograph and Overhead Conductor Rail System. *IEEE Trans. Instrum. Meas.* **2022**, 71. [CrossRef]